J Solid State Electrochem (2011) 15:329–347
DOI 10.1007/s10008-010-1233-3

ORIGINAL PAPER

Simulation of a mixed-conducting membrane-based gas turbine power plant for CO_2 capture: system level analysis of operation stability and individual process unit degradation

Konrad Eichhorn Colombo · Vladislav V. Kharton · Alexandre P. Viskup · Andrei V. Kovalevsky · Aliaksandr L. Shaula · Olav Bolland

Received: 17 November 2009 / Revised: 31 October 2010 / Accepted: 2 November 2010 / Published online: 25 November 2010

Abstract A gas turbine power plant for CO_2 capture, based on oxygen-permeable membranes with mixed ionic-electronic conductivity, was analysed with respect to long-term stability by means of numerical simulation. Due to the attractive transport and physicochemical properties of mixed-conducting $La_2NiO_{4+\delta}$, this nickelate was selected as a prototype membrane material for this application. Experiments showed very slow degradation of $La_2NiO_{4+\delta}$ membranes at oxygen chemical potentials close to atmospheric conditions, which are associated with kinetic demixing and other microstructure-related factors. Interaction with CO_2 in the intermediate temperature range also leads to lower oxygen permeation, whilst increasing oxygen pressure may cause partial phase decomposition and microstructural changes, thus again limiting the range of possible operation conditions. The relevant operational constraints were included in a detailed membrane-based gas turbine power plant model. The membrane performance degradation with time was approximated by a linear function with average rate of 3.3% per 1,000 operation hours. Furthermore, performance deterioration of the gas turbine compressor and turbine were also considered. Simulations revealed that the power plant is substantially affected by degradation of the ceramic membranes and turbomachinery components. The already rather small operating window was further narrowed when compared with a conventional gas turbine power plant. Two different designs of the membrane-based power plant were analysed: (1) with and (2) without additional combustors (afterburners) between the membrane reactor and the gas turbine. Afterburners increase thermal efficiency as well as power output, but also lead to non-negligible CO_2 emissions. In order to have a frame of comparison, results for a conventional gas turbine power plant with degradation of turbomachinery components are also presented. Simulations representing changes in ambient temperature and fuel composition as well as failure incidents were executed to analyse the susceptibility of the gas turbine power plant to external and internal changes.

Keywords Oxygen mixed-conducting membranes · Oxy-combustion · Gas turbine power plant · Lanthanum nickelate membranes · Long-term stability · Performance deterioration · Failure analysis · CO_2 capture and storage

K. Eichhorn Colombo (✉) · O. Bolland (✉)
Department of Energy and Process Engineering,
Norwegian University of Science and Technology,
Kolbjørn Hejes vei 1B,
7491, Trondheim, Norway
e-mail: konrad.eichhorn@ntnu.no

O. Bolland
e-mail: olav.bolland@ntnu.no

V. V. Kharton (✉) · A. V. Kovalevsky · A. L. Shaula
Department of Ceramics and Glass Engineering, CICECO,
University of Aveiro,
3810-193, Aveiro, Portugal
e-mail: kharton@ua.pt

V. V. Kharton · A. P. Viskup · A. V. Kovalevsky
Institute of Physicochemical Problems, Belarus State University,
14 Leningradskaya Str.,
220050, Minsk, Belarus

A. V. Kovalevsky
Separation and Conversion Technology Department,
Flemish Institute for Technological Research (VITO),
2400, Mol, Belgium

A. L. Shaula
Department of Mechanical Engineering, SEG-CEMUC,
University of Coimbra,
3030-788, Coimbra, Portugal

Introduction

Oxygen mixed-conducting membranes (OMCMs) have attracted a great deal of attention in recent years because of their economic as well as environmental advantages. For instance, these membranes can be used as an oxygen production device in gas turbine power plants (GTPPs) for CO_2 capture [1–6]. But depending on their degree of integration, they also represent a fundamental challenge in terms of process design, operability, and long-term stability. These issues have not yet been widely addressed for entire CO_2 capture power processes. Moreover, relatively little research has been conducted on long-term stability issues of OMCMs for energy applications, although a number of relevant publications do exist in the literature (e.g. [6–11]). This is of particular interest for the power plant analysed in this paper since the membranes are exposed to atmospheres containing large amounts of CO_2 and water vapour, both of which may affect the lifetime of the material.

In this work, a multi-disciplinary approach was followed where experimental results on the membranes were incorporated into a detailed membrane-based GTPP model. In order to build a robust and relatively fast model, experimental results used for numerical simulations have been averaged. Consideration of all material specific properties and phenomena is not possible without a full-scale process set-up. Key power plant components were modelled in a spatially distributed manner. The model of the mixed-conducting membrane module is briefly presented in the Appendix. Additional modelling and simulation assumptions can be found in previous works [12, 13].

The present paper is focused on the stability issues of the membrane-based GTPP and is organized as follows. The next section outlines the principles of the membrane-based GTPP as well as relevant degradation and failure mechanisms related to individual process components, in particular the ceramic membranes. Then the processing and measurement procedures and properties of the selected ceramic membranes are briefly addressed. Finally, experimental results for the membrane as well as simulation results for the membrane-based GTPP are presented. A comparison with a conventional GTPP is also provided.

Gas turbine power plants: principles, operation, and maintenance issues

Figure 1 shows the principle of the membrane-based combined cycle power plant in layman terms. The combustor in a conventional GTPP (Fig. 2) is replaced by a membrane reactor [1, 2, 4–6, 14]. After compression in the compressor, the air is fed to the membrane reactor; oxygen is transported through the membranes and enters the recycle loop where combustion with natural gas (assumed to be pure CH_4) takes place in a nitrogen-free atmosphere. The main products are water vapour and CO_2. The gas in the recycle loop serves several purposes: it moderates the combustion temperature, increases the driving force for oxygen transport and keeps the pressure gradient low across the solid walls of the membrane modules and heat exchangers (HXs). A fraction of this stream is bled off from the recycle loop. The compressed air is further heated by means of additional combustors (afterburners) before being fed to the turbine. In the power plant configuration without afterburners, only oxygen-depleted air is emitted to the atmosphere and all the CO_2

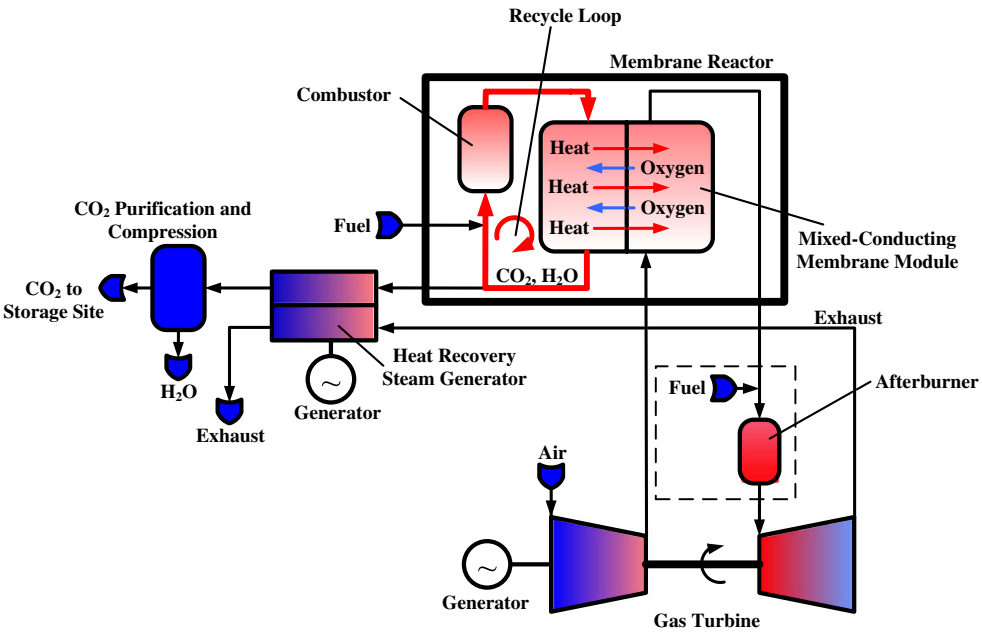

Fig. 1 Principle of the mixed-conducting membrane-based combined cycle power plant with afterburners and subsequent CO_2 conditioning. The temperature profile of process components is indicated throughout the process

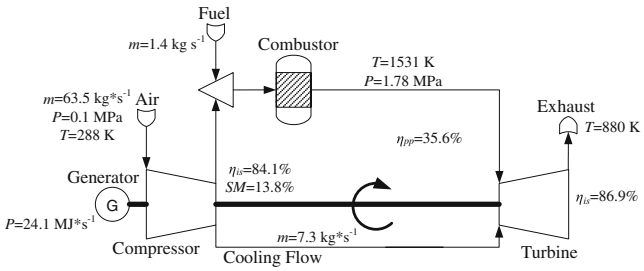

Fig. 2 Conventional gas turbine power plant with some design specifications

present can theoretically be captured. On the other hand, afterburners raise efficiency and power output. Further utilisation of the GT's exhaust gas and CO_2-rich gas in a bottoming steam cycle also increases power plant efficiency and power output. After further cleaning steps, the CO_2 is compressed and transported to a storage site as indicated in Fig. 1 (the analysis including the bottoming steam cycle and the CO_2 conditioning processes can be found in [12]). The process flowsheet in Fig. 3 shows the membrane-based GTPP in more detail. Fuel is introduced into the recycle loop by means of ejectors. The compressed air from the compressor is split, with the majority led through the low-temperature HXs, membrane modules and high-temperature HXs. The use of membrane modules for the entire heat transport, thus replacing the low-temperature HX and high-temperature HX, is not feasible because of stability issues and increased costs. In particular, the membrane modules would be partly operated in a temperature range where stability cannot be maintained. The remainder air is fed to the bleed-gas HX branch and mixed with the oxygen-depleted air coming from the high-temperature HX afterward. A modular design was assumed for the membrane reactor components, indicated by the two different flow manifolds in Fig. 3. The temperature of the oxygen-depleted air is further increased in the afterburners before being fed to the turbine. For sound operation of the membrane-based GTPP (Fig. 3) additional issues must be addressed to maintain the stability of critical process components [12, 13].

The most common cause of performance deterioration in a conventional GTPP is compressor fouling [15–21]. This phenomenon can lead to a decreased surge margin [22, 23] and reduced efficiency as well as total flow rate of the compressor [15–18, 22, 24–26]. But fouling is usually recoverable to some extent [15, 17, 18, 25, 27]. The turbine efficiency decreases due to fouling or erosion [16, 26]. Fouling can be reduced by using an effective filtration system [25]. Such systems however can cause a pressure

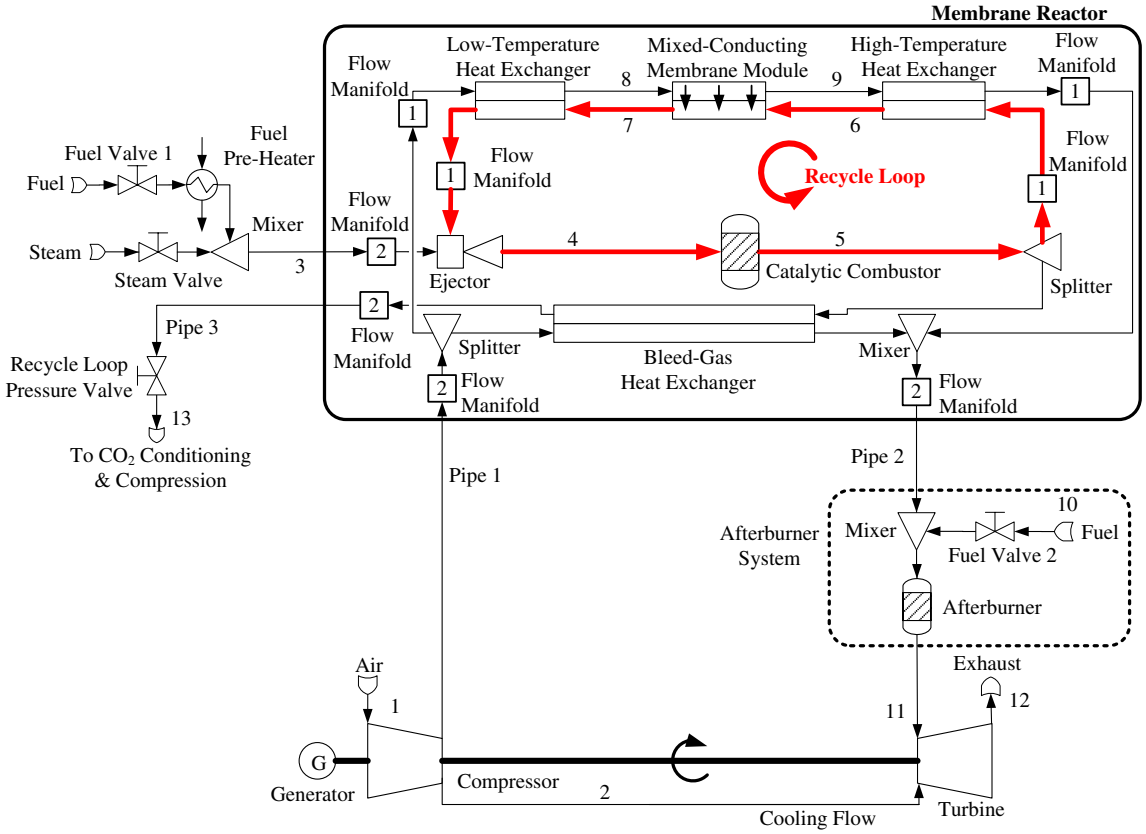

Fig. 3 Membrane-based gas turbine power plant with afterburners

drop leading to reduced power output and efficiency [28]. Degradation rates of turbomachinery components used in this analysis are summarized in Table 1. Further details on degradation of gas turbines can be found in a recently published review [22]. Conventional GTPPs are usually cleaned on a monthly basis, but more frequent washing procedures may be required, for instance on-line washing scheduled after 50 h and off-line washing after 500 h [24, 29]. In an on-line washing procedure, the GT is running at high speed, whereas in an off-line wash, the engine is rotated at 20–50% of design speed [20, 25] with a fuel supply being off [30]. The engine needs to be cooled off to assure that the cleaning solvent reaches all compressor stages and does not evaporate [29]. There are also effective solvents available for on-line washing to partly improve reduced performance due to fouling while the power plant is operating at full load. Hence, the GTPP does not need to be shut down and cooled, and a high availability of the power plant can be maintained. But use of these solvents [31–33] to the membrane-based GTPP can be detrimental to the membrane layer at elevated temperature, whereas pure water-washing is not sufficiently effective [20, 25, 31, 33–35]. An extensive amount of de-ionized or de-mineralized water is needed during the washing process, which may represent an additional economic and logistic constraint for remote power plant locations [36]. Moreover, it should be mentioned that the waste washing agent may also be environmentally hazardous [37]. Bypassing the membrane reactor during the on-line washing procedure is either not recommended from a control point of view, i.e. valves in the main stream should be avoided, or simply not possible because of operational and/or material constraints. The GTPP then needs to be shut down and cooled for off-line washing so that the membranes are not in direct contact with the solvent. For the cleaning of conventional GTPPs, on-line and off-line washing procedures are complementary [20]. For the membrane-based power plant, frequent shut-downs and start-ups are very likely to accelerate degradation.

The combustors in the conventional GTPP and the afterburners in the membrane-based GTPP are, in general, not directly affected by degradation [16, 26, 27, 38]. Due to the lack of available data, degradation of the catalytic combustors in the membrane reactor [12] was also neglected.

The membrane material considered in the present work is intergrowth lanthanum–nickel oxide ($La_2NiO_{4+\delta}$) [39–43] with K_2NiF_4-type structure. This composition and its derivatives exhibit a series of important advantages, namely quite high oxygen permeability, moderate thermal expansion compatible with glass-ceramic sealants and stainless steel, very low chemical-induced stresses and absence of alkaline-earth cations that may promote interaction with gaseous species such as CO_2. In fact, $La_2NiO_{4+\delta}$ exhibit highest oxygen permeation fluxes known for alkaline-earth metal cation-free membrane materials, except for some dual-phase composites. As the performance of OMCMs is improved by reducing the thickness with an appropriate surface modification [1, 44, 45], the dense membrane layer was assumed to be coated onto a porous support (Fig. 4), which partially protects the membrane surface due to mass transport limitations in the pores and to CO_2 displacement from the pores by oxygen transported through the dense layer. The resultant diffusion barrier suppresses CO_2 penetration and increases the oxygen chemical potential at the membrane surface, thus increasing stability of $La_2NiO_{4+\delta}$ and preventing its decomposition. Using the same material for the membrane layer and porous support solves the thermal and chemical expansion mismatch problem [46] and avoids interaction between the membrane components at elevated temperatures. However, use of $La_2NiO_{4+\delta}$ as support material may again lead to limitations associated with possible carbonation. One potential solution considered in this work relates to infiltration of additional catalytically active components forming thin layers on $La_2NiO_{4+\delta}$ surface, both in the pores and on the dense layer surface as indicated in Fig. 4. One should note that the deposition of porous exchange catalysts is necessary for most mixed-conducting materials [40, 42, 44, 47–50], in particular for relatively thin membrane layers [45]. This solution leads to a lower oxygen permeation, which stems from a decreased pore size and higher mass-transfer resistance. In the present work, it was therefore assumed that the additives are only incorporated at those parts of the membrane where high risks for carbonation exist, causing a drop in oxygen flux density of approximately 25%. The

Table 1 Degradation rates of the membrane and turbomachinery components used for modelling

Process unit	Cause of deterioration	Effect of deterioration	Rate [% per 1,000 h]
Compressor	Fouling	Reduction in mass flow of air	1.2 [16, 33]
Compressor	Fouling	Reduction in isentropic efficiency	1.5 [33]
Turbine	Erosion or fouling	Reduction in isentropic efficiency	1.5
Membranes	Surface modification	Reduction in average oxygen flux	3.3

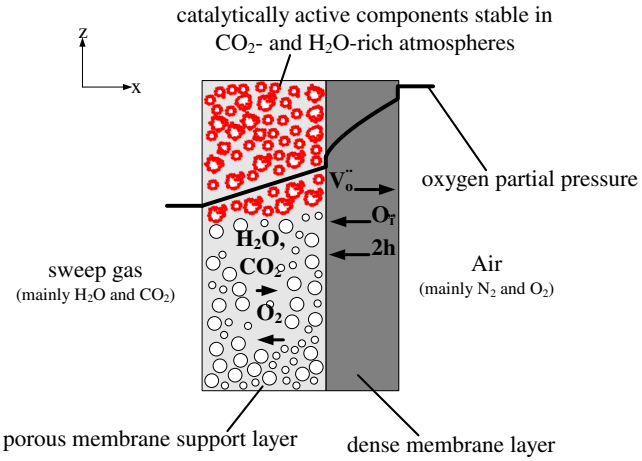

Fig. 4 Schematic drawing of the oxygen transport mechanism and oxygen partial pressure distribution across the dense membrane layer and porous support. The infiltration of additional catalytically active components forming thin layers on $La_2NiO_{4+\delta}$ surface, both in the pores and on the dense layer surface, is also shown

degradation rates of the dense membrane layer and porous support were assumed equal (Table 1).

The mean solid-wall temperature of the membrane modules was approximately 1,264 K, with the hottest parts being at approximately 1,300 K. Heating above 1,323 K should be avoided because of the risk of high-temperature creep, which has been identified as the most restricting property [6] in addition to evaporation of the membrane layer.

It should be noted that numerous other phenomena also have a substantial effect on the long-term stability of ceramic membranes, such as kinetic demixing caused by non-negligible cation mobilities, microstructural changes associated with redox processes, and chemically induced stresses [40, 41, 46, 51–53]. Taking into account the membrane operating conditions that are necessary for the GTPP [6, 12–14], the most critical factors related to the gas composition include high partial pressures of CO_2, H_2O and O_2. The degradation rates associated with these factors were assessed experimentally, as described below. Additional information with respect to material and operational constraints, control strategies as well as start-up and shut-down procedures for the membrane-based power plant can be found elsewhere [12, 13].

Modelling and experimental procedures

The model of the membrane-based and conventional GTPPs were executed in gPROMS [54], an equation-oriented modelling and simulation tool. Physical gas properties were obtained from the physical property package Multiflash [54] using a Soave–Redlich–Kwong equation of state. Experimentally determined physical solid-phase properties for the membrane were represented by nonlinear multi-parameter regression functions [55]. Conservation balances for the spatially distributed parameter system models were discretized by finite difference methods. The approximation of partial derivatives was second order. The whole system was solved by a variable order backward differentiation formula (DASOLV solver) [54]. A general rule for the required calculation time cannot be defined a priori. The solver varies time increments depending on discontinuities and current changes in process variables. The model of the membrane-based GTPP consists of more than 12,000 equations.

Detailed descriptions of the experimental procedures and equipment, used for processing and characterization of dense $La_2NiO_{4+\delta}$ membranes and physicochemical properties of lanthanum nickelate ceramics were published in previous works ([39, 40, 47–50, 56–58] and references cited). The oxygen permeability measurements under ambient total pressure were performed using the electrochemical cells made of yttria-stabilized zirconia solid electrolyte; high-pressure permeation tests were carried out in the stainless steel chamber where a dense ceramic membrane was hermetically sealed onto a metallic tubular support [47]. After all measurements, $La_2NiO_{4+\delta}$ membranes were additionally characterized by X-ray diffraction (XRD) and scanning electron microscopy coupled with energy dispersive spectroscopy (SEM/EDS). For the dilatometric tests, a vertical alumina dilatometer Linseis L75V/1250 was used.

Results and discussion

Oxygen permeability and stability of $La_2NiO_{4+\delta}$ membranes: model input data

In order to justify selection of $La_2NiO_{4+\delta}$ as the model membrane composition, Fig. 5 compares the oxygen permeation fluxes and thermal expansion of several mixed conductors that are considered among the most promising candidates. Although the level of oxygen permeation through $La_2NiO_{4+\delta}$ is lower compared to perovskite-type phases such as $SrCo_{0.8}Fe_{0.2}O_{3-\delta}$ or $La_{0.5}Sr_{0.5}FeO_{3-\delta}$, the cobaltite- and ferrite-based perovskites also exhibit volume changes that are twice as high as $La_2NiO_{4+\delta}$ when heating up to the membrane operating temperatures. Moreover, the presence of alkaline-earth cations is expected to increase reactivity with gaseous species, such as SO_x, due to the very high thermodynamic stability of alkaline-earth sulphates. Sulphur poisoning is of critical importance for all mixed-conducting compositions, including $La_2NiO_{4+\delta}$ [6], and can only be avoided when using a desulphurization

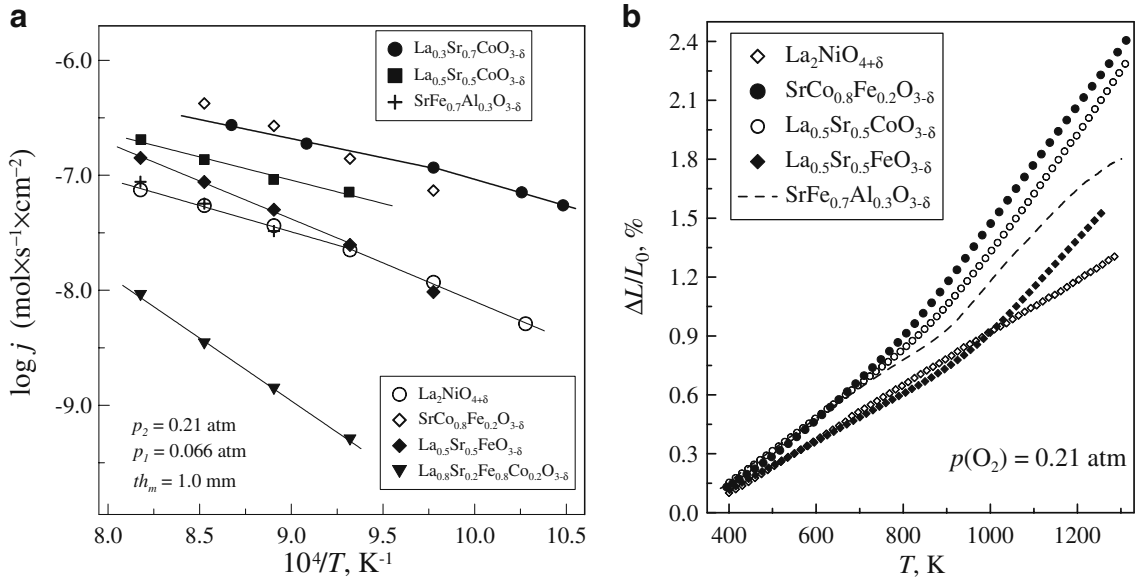

Fig. 5 Comparative data on steady-state oxygen permeation fluxes under fixed oxygen pressure gradient (**a**) and thermal expansion (**b**) of perovskite-related mixed conductors [40, 48–50, 56–58], justifying selection of $La_2NiO_{4+\delta}$ as membrane material. All permeation fluxes correspond to membranes without surface modification. The membrane thickness was 1.00±0.02 mm. Thermal expansion was measured by dilatometry, using the continuous heating regime (3 K/min) in atmospheric air

process. Similar stability problems can be expected in CO_2-containing atmospheres.

Figure 6 presents one example illustrating the degradation of $La_2NiO_{4+\delta}$ membranes in CO_2-containing environments. It displays the variations of specific oxygen permeability, $J(O_2)$ [47, 48], when the membrane permeate side is exposed to a CO_2-containing gas mixture or atmospheric air. The specific permeability is defined as

$$J(O_2) = \frac{j \mathrm{th_m}}{\ln\left(\frac{p_2}{p_1}\right)} \quad (1)$$

where j, $\mathrm{th_m}$, p_2 and p_1 are the oxygen flux density, dense membrane thickness and the oxygen partial pressure at the membrane feed and permeate sides, respectively. $J(O_2)$ is the proportionality coefficient between the flux and oxygen pressure gradient, and reflects transport properties of the membrane during transient periods when both the oxygen flux and its driving force change due to unavoidable experimental uncertainties, such as non-ideal gas mixing and displacement in the measuring chamber. The results shown in Fig. 6 indicate, in particular, a fast and irreversible degradation in CO_2 at 1,023 K. Typical examples of $La_2NiO_{4+\delta}$ membrane degradation rates in CO_2-containing atmospheres are listed in Table 2. At 1,223 K and atmospheric pressure, the presence of CO_2 apparently has no detrimental effect within the limits of experimental error, which is in agreement with thermodynamic data (e.g. [59, 60] and references therein). However, analysis of the thermodynamic properties of lanthanum carbonate and oxycarbonate shows that an opposite situation is likely to take place at the elevated pressure range necessary for the GTPP, even if temperatures are moderately higher than 1,223 K. Note also that the data shown in Fig. 6 might

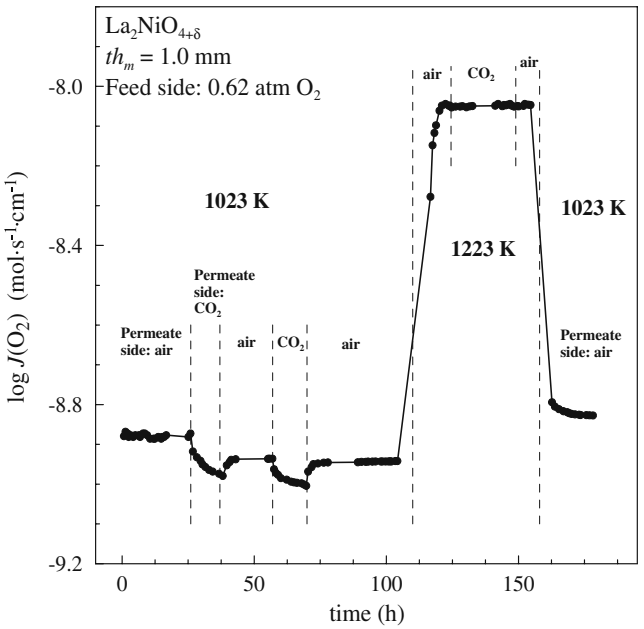

Fig. 6 Time dependence of the specific oxygen permeability of one $La_2NiO_{4+\delta}$ membrane under conditions when the permeate side surface was exposed to atmospheric air or flowing CO_2–O_2–N_2 gas mixture at 1,023 and 1,223 K. The partial pressures of CO_2 and oxygen in the CO_2–O_2–N_2 mixture were 0.47±0.02 and 0.11±0.01 atm, respectively. The oxygen partial pressure at the membrane feed side (p_2) was fixed at 0.62±0.02 atm

Table 2 Examples of time degradation of the oxygen permeation fluxes[a] through $La_2NiO_{4+\delta}$ membranes during the initial period of testing in CO_2-containing atmospheres

T, K	$p(O_2)$, atm		$p(CO_2)$, atm		Time, h	$\Delta j/j_{initial}$, %
	Permeate side	Feed side	Permeate side	Feed side		
1,223	0.11	0.62	0.5	–	50	0
1,173	0.11	0.61	0.5	–	50	0.3
1,073	0.10	0.62	0.5	–	50	17
1,023	0.11	0.62	0.5		50	68
973	0.10	0.64	0.5	–	25	94
1,023	1.0	11.3	–	2	10	53
1,023	1.0	11.3	–	5	10	96
973	1.0	10.9	–	5	10	~100

[a] All data correspond to dense, 1.0-mm-thick membranes without surface modification

suggest the feasibility of thermal cycling to prevent membrane degradation. For instance, a dense $La_2NiO_{4+\delta}$ membrane exposed to CO_2 at 1,023 K exhibited even a ~10% increase in the permeation flux after annealing at 1,223 K. Such an apparent improvement is associated with irreversible changes in the surface layer morphology. Namely, carbonate decomposition enlarges the specific surface area, and leads to the formation of closed pores and microcracks in the surface layer (cf. SEM micrographs shown in Fig. 7a and b). But the range where such temperature cycling is possible for the power plant is very limited due to the high degree of integration with other critical process components. The relatively fast degradation in CO_2 made it necessary to introduce membrane operational limits in addition to the protecting layer, as discussed below.

Another important degradation mechanism of the $La_2NiO_{4+\delta}$ membranes is associated with oxidation at high oxygen chemical potentials [6, 61] and relatively low temperatures, i.e. decomposition of $La_2NiO_{4+\delta}$ into Ruddlesden-Popper nickelates $La_{n+1}Ni_nO_{3n+1\pm\delta}$ ($n>1$) and lanthanum oxide, which may then react with CO_2 or other gaseous species. Figure 8 shows selected experimental data on the permeation at elevated oxygen pressures on the membrane feed side. When the oxygen chemical potentials are close to atmospheric, $La_2NiO_{4+\delta}$ membranes exhibit almost linear dependencies between j and log (p_2/p_1) that means the integral form of the Wagner law is observed. However, increasing p_2 or decreasing p_1 leads to serious deviations. Analysis of the behaviour observed on reducing oxygen pressure showed a more pronounced role of the surface exchange processes, which tend to become the permeation-limiting factor [49]; the fluxes tend to become almost p_1-independent on reduction. In contrast, the dramatic rise of the oxygen fluxes observed at $p_2>10$ atm is caused by oxidation decomposition and resulting microstructural alterations. Indeed, XRD analysis of $La_2NiO_{4+\delta}$ ceramics after high oxygen pressure tests demonstrated the formation of several impurity phases, including $La_4Ni_3O_{10\pm\delta}$ and $LaNiO_{3-\delta}$; traces of secondary phases were also revealed by SEM as illustrated in Fig. 7c. Notice that the level of oxygen ion diffusivity in $La_4Ni_3O_{10\pm\delta}$ and $LaNiO_{3-\delta}$ at elevated oxygen pressures, when the concentration of oxygen vacancies is low if any, is still unknown. However, SEM inspections revealed also substantial microstructural changes, namely an exfoliation of the oxidized surface layer (Fig. 7d) and numerous microcracks. These changes caused by the partial phase decomposition are expected to contribute considerably to the increase in oxygen permeation. As a consequence, the permeation fluxes at high $p(O_2)$ tend to increase with time (Fig. 9). The microstructural changes observed on oxidation are expected to essentially limit the use of $La_2NiO_{4+\delta}$ at elevated oxygen pressures and intermediate temperatures. In light of the thermodynamic data (see [61] and references cited), the lower temperature limit of the nickelate membrane operation at high $p(O_2)$ cannot be decreased below 1,150–1,200 K. In this work, the temperature range of 1,260–1,300 K was considered for the membranes.

Finally, Figs. 7e and 10 illustrate typical degradation processes observed during long-term operation under ambient conditions due to kinetic demixing and resultant microstructural changes. These degradation processes occur substantially more slowly than those associated with the phase decomposition and lead to much smaller changes in the oxygen permeation fluxes, often comparable to the level of experimental errors. The polished and surface-modified membranes (Fig. 10) exhibit qualitatively similar behaviour suggesting that, most likely, main sources of the degradation are related to the membrane bulk. The same conclusion could be drawn from the fact that the average rates of degradation with time, displayed by the polished and modified membranes, are quite similar. Owing to the process complexity and numerous factors influencing

kinetically stagnated cation diffusion in the dense ceramic materials, the time dependencies of the oxygen permeation fluxes are characterized by a relatively poor reproducibility and depend strongly on the initial membrane microstructure. This made it impossible to use complex theoretical models of kinetic demixing. The variations in the oxygen fluxes with time for the long-term stability of the power plant were hence approximated by the simplest of linear models using an average degradation rate. Such an assumption seems quite reasonable because only the first 1,000 h of power plant operation were analysed in this work. Since the typical degradation rates observed experimentally varied in the range 0–4% per 1,000 operation hours at 973–1,223 K, the value of 3.3% per 1,000 h, which is close to the upper possible limit, was selected for simulation (Table 1). Note that Diethelm et al. [62] recently reported a degradation rate of 3.7% per 1,000 h for ferrite-based membranes.

Simulated performance of the membrane-based power plant with and without afterburners: absence of degradation

Figure 11 illustrates the risk of carbonate formation in the membrane modules of the $La_2NiO_{4+\delta}$ membrane-based GTPP without afterburners, expressed by the CO_2 pressure difference between the sweep gas and the defined limit [12] (the modelling results with afterburners have been presented in references [12, 13]). At the sweep gas inlet, the membrane surface may be blocked by carbonates, thus confirming that an extra protection layer should be infiltrated into the porous support (Fig. 4). The length of the porous support with a protective layer is indicated in Fig. 11. As mentioned earlier, this type of protection led to a reduction in the oxygen flux of approximately 25%. Also shown is the oxygen pressure difference between the air and the sweep gas branch and the oxygen flux density. It should be noted that a design case, where no protective layer in the porous support is used and

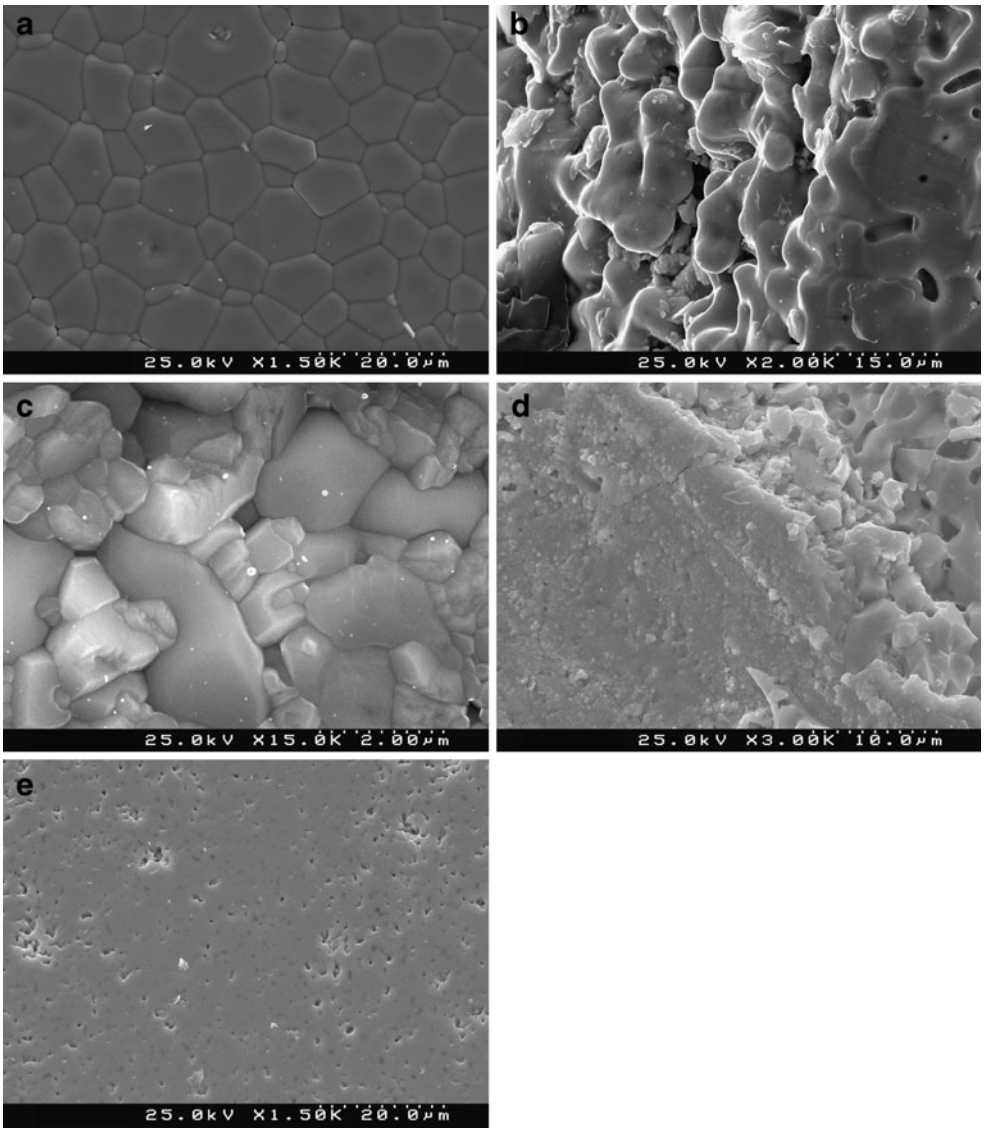

Fig. 7 SEM micrographs showing typical microstructures of $La_2NiO_{4+\delta}$ membranes: **a** after preparation, **b** permeate-side surface after exposure to CO_2-containing atmosphere and thermal cycling, **c** and **d** fractured ceramics after testing at high oxygen pressures; **e** polished feed-side surface after long-term testing at 973 K and atmospheric total and oxygen partial pressures. The image (**c**) illustrates alterations in the membrane bulk microstructure near the feed side where secondary phases were formed. **d** shows an exfoliation of a thick layer formed at the feed-side surface (*left*) from oxidation. The small dark spots in (**e**) correspond to Ni-enriched zones formed due to kinetic demixing and/or oxidation of the feed-side surface at 973 K in air, detected by EDS analysis

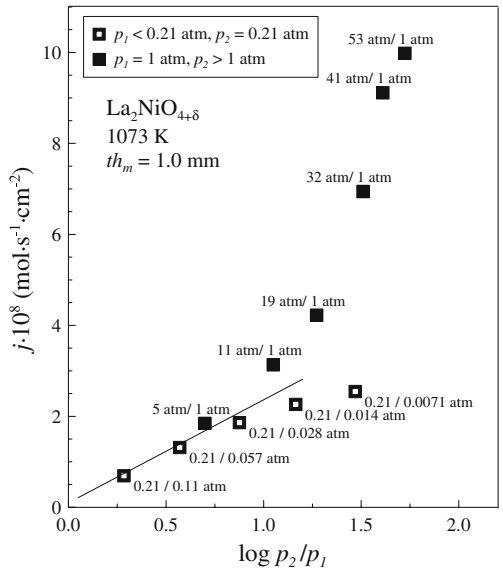

Fig. 8 Oxygen permeation fluxes through dense $La_2NiO_{4+\delta}$ membranes at elevated and moderately reduced oxygen pressures. The deviation from Wagner law (*solid line*) under increasing oxygen pressure is associated with oxidative decomposition and resultant microstructural changes

where process conditions and geometry of the membrane module are such that carbonate formation can be completely avoided, is not feasible. High concentrations of oxygen in the sweep gas (>1.7 mol%) downstream of the catalytic combustors would be necessary to shift the operation conditions into the stable region for all parts of the membranes. Furthermore, increasing the combustion temperature in the catalytic combustors, so that the carbonate formation can be avoided, is also not recommended because the higher temperature limit of the membranes would be exceeded (>1,345 K). Because of higher oxygen concentrations, the performance of the catalytic combustors is expected to improve, but purification requirements for CO_2 capture and compression would also increase, leading to additional power plant efficiency penalties [12]. For the membrane-based power plant without afterburners, modifi-

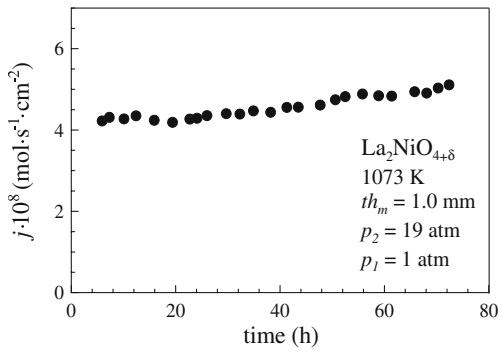

Fig. 9 Typical time dependence of the oxygen permeation fluxes through dense $La_2NiO_{4+\delta}$ ceramics at elevated oxygen pressures. Experimental conditions are given in the legend

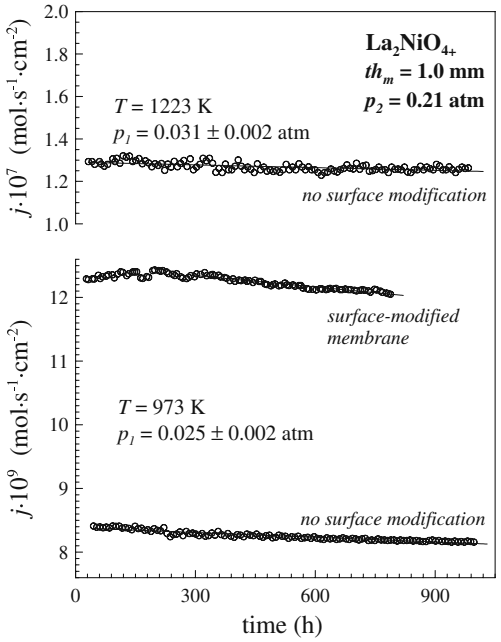

Fig. 10 Examples of the time dependencies of the oxygen permeation fluxes through dense $La_2NiO_{4+\delta}$ ceramics with and without surface modification. For the surface-modified membrane, porous $La_2NiO_{4+\delta}$ layers (~10 mg/cm^2) were applied onto both surfaces, with subsequent infiltration of Pt (loading of ~0.5 mg/cm^2). For the processing conditions, see reference [49]

cations of the membrane modules and HXs length were required to obtain equal design specifications for key variables, i.e. a combustion temperature of 1,473 K and an excess oxygen mole fraction of approximately 1%. Since the difference in turbine inlet temperature differs by approximately 200 K (stream 11 in Fig. 3 and Table 3), considerably less bleed air was needed for cooling the turbine (1.8%; compared to 11.6% for the design with afterburners [12,

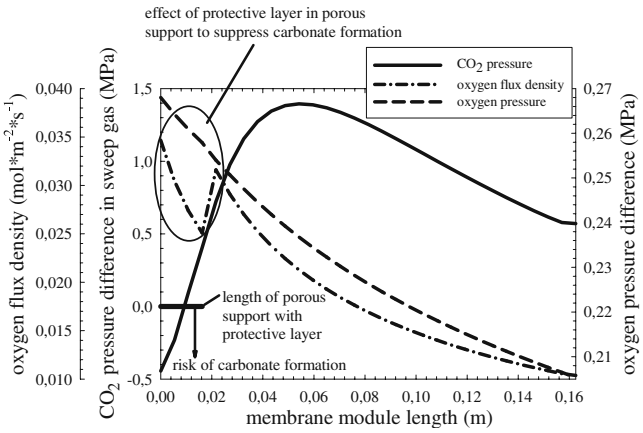

Fig. 11 Simulated risk of carbonate formation (expressed by the difference of the actual CO_2 pressure and the defined limit [12, 13]), oxygen flux density and oxygen pressure difference between air and sweep gas in axial direction for the membrane-based power plant without afterburners

Table 3 Design case results for the membrane-based power plant[a] with (w) and without (wo) afterburners

Stream number	*T*, K		*P*, MPa		Mass flow rate, kg/s		Molar fractions of the gas components (%)									
							N_2		O_2		CH_4		H_2O		CO_2	
	w	wo	w	wo	w	wo	w	wo	w	wo	w	wo	w	wo	w	wo
1	288	288	0.1	0.1	63.5	63.5	79	79	21	21	0	0	0	0	0	0
2	707	697	1.79	1.73	7.3	1.1	79	79	21	21	0	0	0	0	0	0
3	489	480	4	4	1.6	1.4	0	0	0	0	55.8	64.5	44.2	35.5	0	0
4	802	759	1.78	1.7	37.1	37	0	0	8.1	8.6	3.5	3.8	65.8	63.5	22.6	24.1
5	1,473	1,473	1.76	1.69	37.1	37	0	0	1.1	1	0	0	72.8	71.1	26.1	27.9
6	1,330	1,343	1.76	1.68	32.1	32	0	0	1.1	1	0	0	72.8	71.1	26.1	27.9
7	1,258	1,228	1.76	1.68	35.5	35.6	0	0	8.7	9.1	0	0	67.2	65.3	24.1	25.6
8	1,189	1,138	1.77	1.71	47.7	53	79	79	21	21	0	0	0	0	0	0
9	1,258	1,236	1.76	1.71	44.7	50	83.7	83.3	16.3	16.7	0	0	0	0	0	0
10	278	–	1.75	–	0.3	–	0	–	0	–	100	–	0	–	0	–
11	1,531	1,335	1.7	1.7	60.8	60.4	81.7	82.6	15.3	17.4	0	0	2	0	1	0
12	875	749	0.1	0.1	60.8	60.4	81.7	82.6	15.3	17.4	0	0	2	0	1	0
13	710	697	1.75	1.7	5	5	0	0	1.1	1	0	0	72.8	71.1	26.1	27.9

[a] Streams and stream numbers are shown in Fig. 3

13]). The mass flow through the air branch of the membrane modules was higher and the gas temperature of air at the inlet was lower (stream 8 in Fig. 3 and Table 3). The turbine exit temperature was also lower (stream 12 in Fig. 3 and Table 3), which has major implications for the bottoming steam cycle because its efficiency is sensitive to the turbine exit temperature [12]. Further specifications for the two designs can be found in Table 3 and references [12, 13]. It should be emphasized that for both designs the membrane modules were operated close to their temperature limits.

Part-load performance maps for the membrane-based power plant without afterburners

Figure 12 shows the part-load performance maps where the mean solid-wall temperature of the membrane modules was kept close to its design temperature, which had a positive impact on the membrane stability. Furthermore, the pressure in the recycle loop was controlled to minimize the pressure gradient across the solid walls of the membrane and HX modules, i.e. between air and sweep gas. Variable guide vanes (VGVs) in the compressor were used to obtain the demanded power output as well as target temperatures of the membrane modules. Compared to the power plant design with afterburners [12, 13], VGVs could here not be applied to control the turbine exit temperature. Variations in GTPP efficiency, excess oxygen in the catalytic combustors, turbine exit temperature and pressure difference in the mixing section of the ejectors for the membrane-based GTPP without afterburners are shown in Fig. 13. In the design case, the power output was 13.6 MW with an efficiency of 30.9%. The load could be reduced down to 74%, i.e. until the limit of VGVs was reached. This is compared to 19.9 MW power output, an efficiency of 33.4% and a load-reduction capability of 58% for the membrane-based GTPP with afterburners [12, 13].

Conventional power plant: degradation of turbomachinery components

Table 4 compares simulation results of the conventional GTPP with literature data [26], where the mass flow of fuel was kept constant. A fairly good agreement was found. Deviations in the results can be explained by differences in modelling assumptions, for instance with respect to process

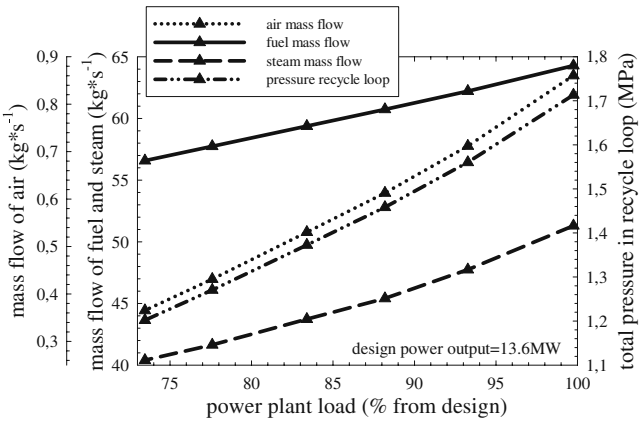

Fig. 12 Steady-state part-load performance maps for the membrane-based power plant without afterburners

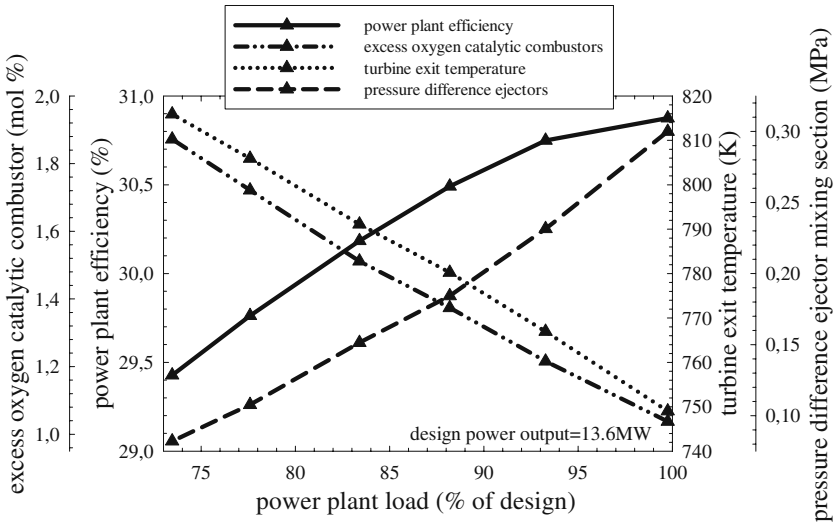

Fig. 13 Calculated power plant efficiency, excess oxygen in the catalytic combustors, turbine exit temperature and pressure difference in the mixing section of the ejectors for the membrane-based power plant without afterburners

component efficiencies that were obtained by performance maps [12, 13]. A reduction in the isentropic efficiency of the turbine was very critical due to its strong effect on the efficiency as well as power output of the GTPP. Assuming a reduction in the isentropic efficiency of the turbine of 5% led to a drop larger than 10% in terms of power plant efficiency and power output. Reduced turbine efficiency had a stronger effect because larger power quantities were involved. An efficiency and power output drop of 85.5% were found for the combined compressor and turbine degradation.

Membrane-based power plant with and without afterburners: membrane degradation

Figure 14 shows the change in the excess oxygen mole fraction in the catalytic combustors for the GTPP with and without afterburners at full load due to degradation of the membranes. For the simulations the mass flow of fuel and steam as well as pressure in the recycle loop were kept at their design value. The effects were similar and severe for both power plant designs. After 1,000 operating hours the excess oxygen mole fraction in the catalytic combustors was less than 0.7 mol% (0.5 mol% was assumed to be the limit where stable combustion conditions can be maintained [12, 13]).

It was found earlier [12, 13] that the excess oxygen concentration in the combustors can be the limiting factor for the membrane-based GTPP with afterburners in terms of part-load operation. Figure 15 shows the large drop in maximum achievable load-reduction capability while keeping the oxygen mole fraction in the catalytic combustors at the 0.5% limit and the mean solid-wall temperature of the membrane modules at the design value of approximately 1,264 K. In this respect, the CO_2 capture rate decreased because both the mass flow of fuel to the catalytic combustors decreased and that of the afterburners increased, as shown in Fig. 15.

Comparison of the conventional and membrane-based power plant with afterburners: degradation of turbomachinery components

Table 5 summarizes the simulation results for efficiency, power output and turbine exit temperature for the conventional and membrane-based GTPP with afterburners when

Table 4 Comparison of simulation results with respect to the turbine exit temperature, efficiency and power output for the conventional power plant, operating at fixed mass flow of fuel and variable turbine exit temperature, with literature data [26]

Source of degradation	Reduction, %	Turbine exit temperature [%]		Efficiency [%]		Power output [%]	
		Reference [26], design, 871 K	This work, design, 880 K	Reference [26], design, 35.6%	This work, design, 35.6%	Reference [26], design, 165.9 MW	This work, design, 24.1 MW
Reduced isentropic efficiency of turbine	−5	~104.3	103.9	~88.5	89.3	~88.4	89.3
Reduced isentropic efficiency of compressor and turbine	−5 (both)	~104.5	105.2	~85.2	85.5	~83.7	85.5

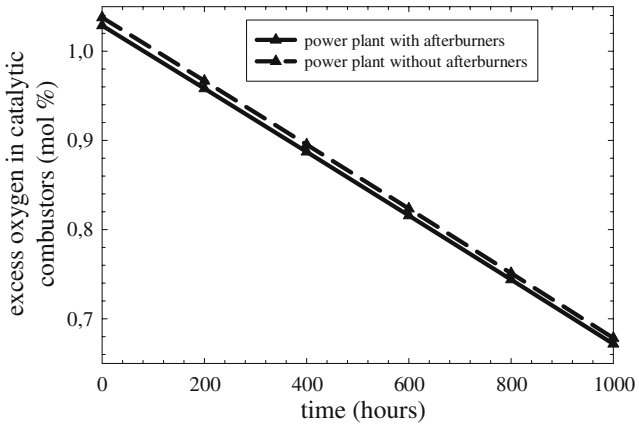

Fig. 14 Reduction in excess oxygen mole fraction in the catalytic combustors of the membrane-based power plant with and without afterburners at full load due to degradation of the membranes. The mass flow of fuel and steam as well as the pressure in the recycle loop were kept at their design values

degradation of turbomachinery components occurs. The responses of both power plants are similar. The corresponding mean solid-wall temperature of the membrane modules and the excess oxygen in the catalytic combustors is shown in Table 6. The temperature of the membrane modules at the sweep gas inlet for cases 4 and 8 was approximately 1,316 K, hence close to the specified limit. The increased average temperature of the membrane modules leads to higher oxygen fluxes and consequently to higher excess oxygen concentrations in the catalytic combustors. On one hand, this behaviour is expected to improve the combustion stability, but on the other hand, the power consumption for CO_2 conditioning will be higher.

Performance of the membrane-based power plant with afterburners: degradation of the membranes and turbomachinery components

Table 7 illustrates the effects of membrane degradation alone (case 9), and in conjunction with degradation of the turbomachinery (cases 10–16). The effect of membrane degradation on efficiency, power output and turbine exit temperature alone was very small, but a reduced oxygen flux had major consequences for the performance of the catalytic combustors. For most cases the oxygen concentration drops, in particular for cases 9 and 13 with <0.7 mol%.

Membrane-based plant with afterburners: changes in ambient conditions and fuel composition

Table 8 lists the results for key variables of the membrane-based power plant with afterburners for the case when changes in ambient temperature as well as composition in fuel occur. The mass flow of the two fuel streams as well as steam to the ejectors and the pressure in the recycle loop were kept at their design values. When the ambient temperature increased by 15 K, the higher temperature limit for some parts of the membrane module was exceeded, which can lead to high-temperature creep [6]. High oxygen concentrations are assumed to have a positive effect on combustion stability, but the power consumption

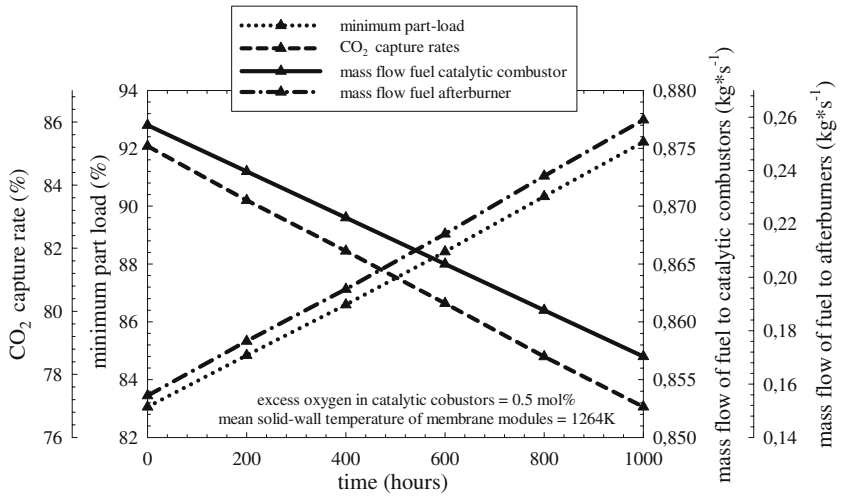

Fig. 15 Minimum achievable part-load of the membrane-based power plant with afterburners after degradation of the membrane modules for the load-control strategy without variable guide vanes and corresponding CO_2 capture rates. The turbine exit temperature was allowed to vary. The mean solid-wall temperature of the membrane modules was kept nearly constant. The excess oxygen in the catalytic combustors was the constraining factor with a limit of 0.5 mol%. The corresponding mass flow of fuel to the catalytic combustors in the membrane reactor and afterburners are also shown

Table 5 Efficiency, power output and turbine exit temperature of the conventional and membrane-based power plant with afterburners after 1,000 h of operation[a]

Sources of degradation	Efficiency, %		Power output, MW		Turbine exit temperature, K	
	Conventional	Membrane based	Conventional	Membrane based	Conventional	Membrane based
(1) Design without degradation	35.6	33.4	24.1	19.9	880	875
(2) Reduced isentropic efficiency of compressor	35.2	33	23.8	19.6	883	878
(3) Reduced mass flow into compressor	35.6	33.5	24.1	19.9	886	883
(4) Cases (2) and (3) combined	35.2	33.1	23.8	19.7	890	886
(5) Reduced isentropic efficiency of turbine	34.4	32.2	23.3	19.2	890	886
(6) Cases (2) and (5) combined	34	31.8	23.1	18.9	894	889
(7) Cases (3) and (5) combined	34.4	32.4	23.3	19.2	897	893
(8) Cases (4) and (5) combined	34.1	32	23	19	900	897

[a] The degradation rates are specified in Table 1; further design specifications can be found in Table 3 and references [12, 13]

for CO_2 conditioning will also increase. For a temperature drop of 15 K, some parts of the membrane approach the lower temperature limit. A similar effect was obtained when assuming a fuel composition of 95% methane with the balance being nitrogen (pure CH_4 was assumed for the base case). In addition, if some membrane parts without the protective layer are exposed to carbonate formation, a rapid degradation can be expected. Note that natural gas itself may also include substantial concentrations of CO_2 [63], which will further increase the risk of degradation. The importance of Fig. 16 lies in the fact that even inert chemical species that dilute the fuel have a great effect on performance and stability. The excess oxygen concentration for a temperature drop of 15 K, and also for changes in fuel composition, reached very critical values (<0.3 mol%). Stable combustion is thus assumed to be not maintainable. As a result, controllers must adjust process conditions to compensate for changes in ambient conditions as well as possible variations in fuel composition.

Failure response of the membrane-based power plant with afterburners

Figure 17a shows the response of the membrane-based power plant after a total failure of the fuel supply to the afterburners. The mass flow of fuel and steam to the catalytic combustors and the pressure in the recycle loop were kept constant. The power output and efficiency decreased rapidly. The excess oxygen concentration dropped well below the limit where stable combustion could be maintained. The temperature of the membrane modules decreased. Both effects result in a higher risk of carbonate formation. The simulations reveal, again, that parts of the membrane layer that were not stabilized by a protective layer can be rapidly poisoned due to carbonation. The turbomachinery reached a new equilibrium point with a surge margin of approximately 26%. This matching between turbomachinery and membrane reactor leads to an average pressure difference of approximately 0.16 MPa

Table 6 Mean solid-wall temperature of the membrane modules and excess oxygen in the catalytic combustors in the membrane-based power plant with afterburners after 1,000 h of operation[a]

Sources of degradation	Mean solid-wall temperature of membrane modules, K	Excess oxygen in catalytic combustors, mol%
(1) Design without degradation	1,264	1.03
(2) Reduced isentropic efficiency of compressor	1,271	1.22
(3) Reduced mass flow into compressor	1,278	1.26
(4) Cases (2) and (3) combined	1,285	1.45
(5) Reduced isentropic efficiency of turbine	1,264	1.03
(6) Cases (2) and (5) combined	1,271	1.22
(7) Cases (3) and (5) combined	1,278	1.26
(8) Cases (4) and (5) combined	1,285	1.45

[a] The degradation rates are specified in Table 1; further design specifications can be found in Table 3 and references [12, 13]

Table 7 Efficiency, power output, turbine exit temperature, mean solid-wall temperature and excess oxygen in the catalytic combustors in the membrane-based power plant with degradation of the turbomachinery components after 1,000 h of operation[a]

Source of performance loss	Efficiency, %	Power output, MW	Turbine exit temperature, K	Mean solid-wall temperature of membrane modules, K	Excess oxygen in catalytic combustors, mol%
(9) Reduced oxygen flux through the membrane	33.4	19.9	875	1,262	0.672
(10) Cases (2) and (9) combined	33	19.6	878	1,269	0.854
(11) Cases (3) and (9) combined	33.5	19.9	883	1,276	0.904
(12) Cases (4) and (9) combined	33.1	19.7	886	1,283	1.084
(13) Cases (5) and (9) combined	32.2	19.2	885	1,262	0.672
(14) Cases (6) and (9) combined	31.8	18.9	888	1,269	0.854
(15) Cases (7) and (9) combined	32.3	19.2	893	1,276	0.904
(16) Cases (8) and (9) combined	31.9	19	896	1,283	1.084

[a] The degradation rates are specified in Table 1; further design specifications can be found in Table 3 and references [12, 13]

between the air and the sweep gas branch of the monoliths, which was above the specified limit of 1 bar [12, 13]. The monoliths are therefore at high risk to break.

Figure 17b displays the response of the membrane-based GTPP with afterburners after a failure of the recycle loop pressure valve, for which a pressure drop of 0.5 MPa was assumed. The drop in power output and efficiency of the new steady state was small. The excess oxygen reached approximately 3 mol%. It is expected that such a large increase of excess oxygen will also have a negative effect on the combustion characteristics. Due to the high oxygen concentration in the sweep gas and increased temperature of the membrane reactor components, the risk of carbonate formation decreased. The SM of the compressor remained close to its design value. The change in the recycle loop pressure had a minor effect on the pressure characteristics of the turbomachinery. Conditions in the air branches of the membrane reactor were not altered much. However, the sudden drop in the recycle loop pressure led to a large pressure gradient across the monoliths of approximately 0.5 MPa, which was well above the specified maximum limit. Mechanical stability can hence not be ensured.

Table 8 Effect of changes in ambient temperature and fuel composition on the performance of the membrane-based power plant with afterburners

Variables	Base case (fuel, 100% methane; ambient temperature, 288 K)	Ambient temperature +15 K	Ambient temperature −15 K	Fuel composition, 95% CH_4, 5% N_2
Power output [MW]	19.9	19.3	20.4	18.7
Power plant efficiency, %	33.4	32.5	34.3	32.9
Mean solid-wall temperature of membrane modules, K	1,264	1,303	1,225	1,215
Maximum temperature of membrane modules, K (limit, 1,323 K [12, 13])	1,299	1,337	1,261	1,252
Minimum temperature of membrane modules, K (limit, 1,173 K [12, 13])	1,230	1,271	1,189	1,179
Turbine inlet temperature, K	1,531	1,562	1,500	1,490
Turbine exit temperature, K	875	893	858	851
Excess oxygen in catalytic combustors, mol% (limit, 0.5% [12, 13])	1.1	2.2	0.07	0.26
Pressure difference in mixing section of ejectors, MPa (limit, 0.1 MPa [12, 13])	0.3	0.34	0.26	0.31
Compressor surge margin, % (limit, 5% [12, 13])	15.4	14.3	16.7	16.8

The mass flow of fuel to the catalytic combustors and afterburners, steam to the ejectors and pressure in recycle loop were kept constant

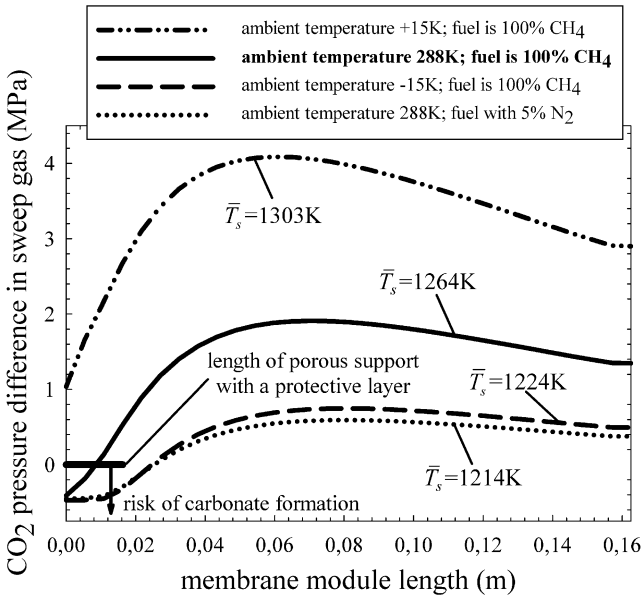

Fig. 16 Effect on the risk of carbonate formation for the membranes for changes in ambient temperature and fuel composition for the membrane-based power plant with afterburners. The length of the membrane support where a protective layer was incorporated is indicated in the *lower left part*. The mean solid-wall temperature of the membrane modules $(\bar{T}_s)$ is also shown

Figure 17c shows the response of the membrane-based power plant after a failure of VGVs in the compressor giving a mass flow reduction of 2.5%. The new steady state of the power output and efficiency were close to the design value. The temperature of the membrane reactor components increased since the fuel supply was kept constant. At the sweep gas entry of the membrane modules the higher temperature limit was exceeded. High-temperature creep will therefore be likely to occur, as indicated in Fig. 17c. The higher temperature however reduced the risk of carbonate formation. The mean oxygen flux in the membrane modules increased and higher oxygen concentrations in the sweep gas of approximately 1.6 mol% were obtained. The surge margin of the compressor was only slightly reduced and the pressure difference between the monoliths remained within the limit.

Conclusions

A mixed-conducting membrane-based gas turbine power plant was analysed with respect to material and operational stability by means of an interdisciplinary and multi-level (time and spatial domain) modelling approach, indicating the importance to introduce materials science and electrochemistry-related parameters into process engineering. Degradation rates of the membrane layers were experimentally obtained and incorporated into a detailed power plant model. Additionally, degradation rates for the compressor and turbine, found in the open literature, were also included. Lanthanum nickelate ($La_2NiO_{4+\delta}$) was selected as a suitable material because of its attractive transport and physiochemical properties. Experiments for the stand-alone ceramic membranes revealed a significant degradation as a result of kinetic demixing and other microstructure-related factors. For the sake of simplicity, a constant degradation rate for the membranes of 3.3% per 1,000 h was assumed in the simulations of the membrane-based GTPP. In conjunction with degradation of turbomachinery components, the operating line was substantially shifted and could quickly bring the membrane-based GTPP into an unstable operation regime. This underlines the necessity of considering critical (power) process components, such as the membrane modules, on a system level rather than individually.

It is important to mention that a shift in operating conditions due to degradation of one process component can result in accelerated degradation of others. For instance, in addition to the risk of flame-out when the excess oxygen in the catalytic combustors falls below the limit, gaseous species such as carbon monoxide may be produced, which in turn are highly reactive with the membranes and further accelerate their degradation.

Standard measures to suppress performance deterioration in conventional GTPPs, such as solvent-based on-line washing, are not likely to be applicable for the membrane-based GTPP, due to the possible interaction between solvent and membrane material. The power plant then needs to be shut down and cooled to avoid direct contact between the solvent and the membranes. However, frequent start-ups and shut-downs are expected to increase degradation rates and the risk of failures in addition to financial penalties for the power plant operator.

Seemingly small changes in the process design, i.e. when afterburners were not used, were found to have a large effect on power output, efficiency and load-reduction capability. The load could only be reduced to approximately 74% that means until the limit of VGVs was reached (compared to 58% for the membrane-based GTPP with afterburners). Moreover, the turbine exit temperature remained uncontrolled, which has major implications for the bottoming steam cycle in a combined cycle power plant.

Changes in ambient temperature as well as fuel composition were found to have a substantial negative impact on the operation and stability of the membrane-based GTPP. As a result, even though the power plant may be located in an area with a benign climate, controllers must not only account for a shift in the operating line due to degradation, but also for external changes, such as ambient temperature variations. This is also the case for conventional power plants. But for the membrane-based GTPP, such off-design conditions are much more pronounced due to several highly critical process components. Furthermore,

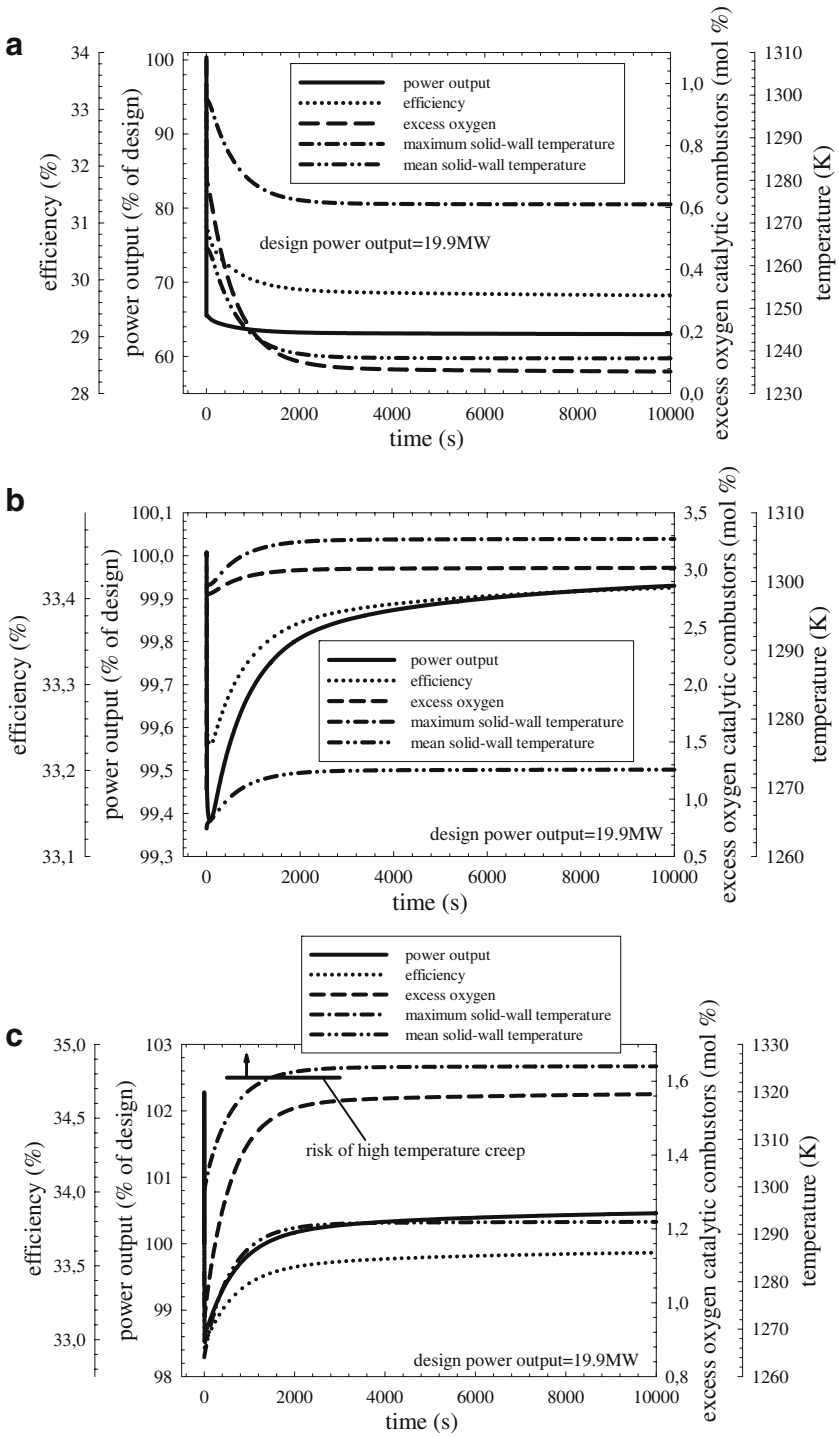

Fig. 17 Response of the membrane-based power plant with afterburners with respect to power output, power plant efficiency, excess oxygen in the catalytic combustors and two characteristic temperatures of the membrane modules, i.e. maximum and mean solid-wall temperature: **a** after a complete failure of the afterburner valves where the fuel supply breaks down (mass flow of fuel drops to approximately zero); **b** after a failure of the recycle loop valve where the pressure in the recycle loop drops (−5 bar); **c** after a failure of the variable guide vanes in the compressor leading to a drop of the mass flow of air (−2.5%)

the shift of operation conditions due to degradation and changes in ambient conditions may also be strongly counteractive, which in turn could lead to faster performance deterioration.

The transient simulation of failure incidents revealed a rather poor response of the membrane-based GTPP. All malfunctions considered in this paper have a detrimental effect on membrane reactor components.

Finally, the membrane-based GTPP showed relatively good performance in terms of efficiency and power output when compared to a conventional GTPP. Nevertheless, the former has considerably more potential sources of degradation and failure.

Long-term stability improvement of the membrane-based GTPP by means of changes in design and/or process conditions is limited. The risk of carbonate poisoning could be reduced when allowing for higher excess oxygen

concentrations in the catalytic combustors. Higher oxygen permeation rates, and thus increased excess oxygen concentrations, could be obtained when using membrane materials that have higher oxygen permeation rates than $La_2NiO_{4+\delta}$. However, many of these highly permeable materials also show high reactivity with gaseous species such as SO_x in addition to high volumetric changes when heating up to the membrane operating temperatures. A change of the membrane module geometry is also very limited. An extension of the membrane modules to increase the oxygen concentration could lead to operating conditions where parts of the membrane module are operated beyond the maximum or minimum temperature limit, respectively. Further improvements of the membranes and other critical process components are therefore required to meet the demand for high performance and an economically viable lifetime for energy applications.

Acknowledgements This publication forms a part of the BIGCO2 project, which has been undertaken as a part of the strategic Norwegian research programme Climit. The authors acknowledge the partners for their support: Statoil, GE Global Research, Statkraft, Aker Clean Carbon, Shell, TOTAL, ConocoPhillips, ALSTOM, the Research Council of Norway (178004/I30 and 176059/I30), Gassnova (182070) and FCT, Portugal (PTDC/CTM/64357/2006 and SFRH/BPD/28913/2006). Experimental assistance and helpful discussions provided by V.N. Tikhonovich and P.F. Kerko are also gratefully acknowledged. The editor and reviewers are acknowledged for their valuable comments on the paper.

Appendix

The oxygen flux was modelled by using an approximate of Wagner's equation [64]:

$$j = \frac{c_0 D_0}{4\mathrm{th_m} n}\left[p_2^n - p_1^n\right] \tag{2}$$

Despite its simplifications, this semi-empirical equation well describes the situations where oxygen transport is limited by both surface exchange and bulk ionic conduction, as typical for La_2NiO_4-based materials [42, 43].

The gas phase energy balance for air and sweep gas reads [12, 13]

$$\rho_g c_{p,g}\left(\frac{\partial T_g}{\partial t} + v_g \frac{\partial T_g}{\partial z}\right) = \alpha h_f\left(T_s - T_g\right) \tag{3}$$

using the following boundary condition at the inlet:

$$T_g\big|_{\mathrm{in}} = T_g^0 \tag{4}$$

The energy balance for the solid wall (dense membrane layer and porous support) is [12, 13]:

$$\rho_s c_{p,s}\frac{\partial T_s}{\partial t} = \lambda_s \frac{\partial^2 T_s}{\partial z^2} + \alpha \sum_{k=1}^{2} h_{f,k}\left(T_{g,k} - T_s\right) \tag{5}$$

in conjunction with

$$\left.\frac{\partial T_s}{\partial z}\right|_{\mathrm{in,out}} = 0 \tag{7}$$

where the indices in and out correspond to the inlet and outlet, respectively.

The species conservation balance for the *i*th species is [12, 13]:

$$\frac{\partial C_i}{\partial t} + v_g \frac{\partial C_i}{\partial z} = \pm \frac{4}{w} j \tag{6}$$

with the corresponding boundary conditions:

$$C_i\big|_{\mathrm{in}} = C_i^0 \tag{8}$$

Please note that the right hand side of Eqs. 6 will be zero for all species but oxygen.

Initial conditions for all differential equations are given by the steady-state assumption.

List of symbols and units

Symbol	Units	Quantity
C	$\mathrm{mol\,m^{-3}}$	Gas concentration
c_0	$\mathrm{mol\,m^{-3}}$	Concentration of mobile oxygen anions
c_p	$\mathrm{J\,kg^{-1}\,K^{-1}}$ or $\mathrm{J\,mol^{-1}\,K^{-1}}$	Heat capacity at constant pressure
D_0	$\mathrm{m^2\,s^{-1}}$	Oxygen self-diffusion coefficient
h_f	$\mathrm{J\,s^{-1}\,m^{-2}\,K^{-1}}$	Heat transfer coefficient
j	$\mathrm{mol\,m^{-2}\,s^{-1}}$	Oxygen flux density
$J(\mathrm{O_2})$	$\mathrm{mol\,m^{-1}\,s^{-1}}$	Specific oxygen permeability
m	$\mathrm{kg\,s^{-1}}$	Mass flow
n	–	Constant
P	Pa or atm, $\mathrm{J\,s^{-1}}$	Total pressure, power
p	Pa or atm	Partial pressure
SM	–	Gas turbine compressor surge margin
T	K	Temperature
t	s	Time
$\mathrm{th_m}$	m	Dense membrane layer thickness
v	$\mathrm{m\,s^{-1}}$	Fluid velocity
w	m	Channel width of the membrane and heat exchanger monolith
z	m	Spatially distributed variable in axial direction
α	$\mathrm{m^2/m^{-3}}$	Area-to-volume ratio of the monolith
η	–	Efficiency

λ	$Js^{-1}m^{-1}K^{-1}$	Thermal conductivity
ρ	kgm^{-3}	Density
Subscript indices		
g		Gas phase
i		Gas species
in, out		Inlet and outlet conditions
is		isentropic
k		Sweep gas or air
pp		Power plant
s		Solid wall

References

1. Bose AC (ed) (2009) Inorganic membranes for energy and fuel applications. Springer, New York
2. Bruun T, Gronstad, L, Kristiansen K, Werswick B, Linder U (2005) US patent application 20050053878
3. Drioli E, Giorno L (eds) (2009) Membrane operations: innovative separations and transformations. Wiley-VCH, Weinheim
4. Griffin T, Sundkvist SG, Åsen K, Bruun T (2005) J Eng Gas Turbines Power 127:81–85
5. Hamrin S (2010) US patent application 20100126137
6. Sundkvist SG, Julsrud S, Vigeland B, Naas T, Budd M, Leistner H, Winkler D (2007) Int J Greenhouse Gas Control 1:180–187
7. Benson SJ, Waller D, Kilner JA (1999) J Electrochem Soc 146:1305–1309
8. Carolan MF, Dyer PN, Labar JM, Thorogood RM (1993) US patent 5240473
9. Kaus I, Wiik K, Krogh B, Dahle M, Hofstad KH, Aasland S (2007) J Am Ceram Soc 90:2226–2230
10. Schlehuber D, Wessel E, Singheiser L, Markus T (2010) J Membrane Sci 351:16–20
11. Waindich A, Möbius A, Müller M (2009) J Membrane Sci 337:182–187
12. Eichhorn Colombo K, Bolland O, Kharton VV, Stiller C (2009) Energ Environ Sci 2:1310–1324
13. Eichhorn Colombo K, Kharton VV, Bolland O (2010) Energy Fuel 24:590–608
14. Linder U, Eriksen E, Asen K (2004) US patent application 20040011048
15. Aker GF, Saravanamuttoo HIH (1989) J Eng Gas Turbines Power 111:343–350
16. Diakunchak IS (1992) J Eng Gas Turbines Power 114:161–168
17. Gülen SC, Griffin PR, Paolucci S (2002) J Eng Gas Turbines Power 124:910–921
18. Lakshminarasimha AN, Boyce MP, Meher-Homji CB (1994) J Eng Gas Turbines Power 116:46–52
19. Leusden CP, Sorgenfrey C, Dümmel L (2004) J Eng Gas Turbines Power 126:763–769
20. Mund FC, Pilidis P (2006) J Eng Gas Turbines Power 128:344–353
21. Seddigh F, Saravanamuttoo HIH (1991) J Eng Gas Turbines Power 113:595–601
22. Bons JP (2010) J Turbomachinery 132:0210041–02100416
23. Spakovszky ZS, Gertz JB, Sharma OP, Paduano JD, Epstein AH, Greitzer EM (2000) J Turbomachinery 122:477–484
24. Caguiat DE (2003) J Turbomachinery 125:482–488
25. Schneider E, Bussjaeger SD, Franco S, Therkorn D (2010) J Eng Gas Turbines Power 132:062001
26. Zwebek A, Pilidis P (2003) J Eng Gas Turbines Power 125:651–657
27. Kurz R, Brun K (2001) J Eng Gas Turbines Power 123:70–77
28. Sánchez D, Chacartegui R, Becerra JA, Sánchez T (2009) Proc IME J Power Energ 223:467–476
29. Rao PNS, Naikan VNA (2008) J Eng Gas Turbines Power 130:0218011–0218015
30. Walsh PP, Fletcher P (2004) Gas turbine performance, 2nd edn. Blackwell Publ, Malden
31. Amiran MC (2001) US patent 6310022
32. Koch KW, Smith DT, Hughes MD, Urbas T (2007) US patent 7185663
33. Woodson JB, Cooper LA, White HM, Fischer GC (1989) US patent 4808235
34. Boyce MP, Gonzalez F (2007) J Eng Gas Turbines Power 129:114–122
35. Stalder JP (2001) J Eng Gas Turbines Power 123:363–370
36. Kohler RW, Wagner T (2010) US patent application 20100147330
37. Hjerpe CJ, Asplund P (2006) US patent application 20060081521
38. Kurz R, Brun K, Wollie M (2009) J Eng Gas Turbines Power 131:0624011–0624017
39. Kharton VV, Viskup AP, Naumovich EN, Marques FMB (1999) J Mater Chem 9:2623–2629
40. Kharton VV, Shaula AL, Snijkers FMM, Cooymans JFC, Luyten JJ, Yaremchenko AA, Valente AA, Tsipis EV, Frade JR, Marques FMB, Rocha J (2005) J Membrane Sci 252:215–225
41. Larring Y, Bredesen R, Nordby T, Grande T, Fontaine ML (2007) Ann Chim-Sci Mater 32:197–212
42. Smith JB, Norby T (2006) J Electrochem Soc 153:233–238
43. Vigeland B, Glenne R, Breivik T, Julsrud S (2003) US patent 6503296
44. Hendriksen PV, Larsen PH, Mogensen M, Poulsen FW, Wiik K (2000) Catal Today 56:283–295
45. Sammells AF, Mundschau MV (eds) (2006) Nonporous inorganic membranes for chemical processing. Wiley-VCH, Weinheim
46. Atkinson A, Ramos TMGM (2000) Solid State Ion 129:259–269
47. Kharton VV, Yaremchenko AA, Kovalevsky AV, Viskup AP, Naumovich EN, Kerko PF (1999) J Membrane Sci 163:307–317
48. Kharton VV, Kovalevsky AV, Yaremchenko AA, Figueiredo FM, Naumovich EN, Shaulo AL, Marques FMB (2002) J Membrane Sci 195:277–287
49. Shaula AL, Naumovich EN, Viskup AP, Pankov VV, Kovalevsky AV, Kharton VV (2009) Solid State Ion 180:812–816
50. Tsipis EV, Patrakeev MV, Kharton VV, Yaremchenko AA, Mather GC, Shaula AL, Leonidov IA, Kozhevnikov VL, Frade JR (2005) Solid State Sci 7:355–365
51. Atkinson A, Selçuk A (2000) Solid State Ion 134:59–66
52. Lein HL, Wiik K, Grande T (2006) Solid State Ion 177:1587–1590
53. Vente JF, Haije WG, Rak ZS (2006) J Membrane Sci 276:178–184
54. gPROMS Advanced process modelling software (2009) www.psenterprise.com
55. DataFit Curve fitting and data plotting software (2006) www.curvefitting.com
56. Kharton VV, Kovalevsky AV, Viskup AP, Shaula AL, Figueiredo FM, Naumovich EN, Marques FMB (2003) Solid State Ion 160:247–258
57. Kharton VV, Kovalevsky AV, Avdeev M, Tsipis EV, Patrakeev MV, Yaremchenko AA, Naumovich EN, Frade JR (2007) Chem Mater 19:2027–2033
58. Yaremchenko AA, Kharton VV, Avdeev M, Shaula AL, Marques FMB (2007) Solid State Ion 178:1205–1217

59. Kobayashi K, Matsushita Y, Igawa N, Izumi F, Nishimura C, Miyoshi S, Oyama Y, Yamaguchi S (2008) Solid State Ion 179:2209–2215
60. Shirsat AN, Ali M, Kaimal KNG, Bharadwaj SR, Das D (2003) Thermochim Acta 399:167–170
61. Bannikov DO, Cherepanov VA (2006) J Solid State Chem 179:2721–2727
62. Diethelm S, Bayraktar D, Graule T, Holtappels P, Van herle J (2009) Solid State Ion 180:857–860
63. Häring HW (ed) (2007) Industrial gases processing. Wiley-VCH, Weinheim
64. Gellings PJ, Bouwmeester HJM (eds) (1997) The CRC handbook of solid state electrochemistry. CRC Press, Boca Raton